

Clinical drug resistance linked to inter-convertible phenotypic and functional states of tumor-propagating cells in multiple myeloma

Aristeidis Chaidos^{1,2}, Chris P Barnes³, Gillian Cowan¹, Philippa C May², Valeria Melo²,
Evdoxia Hatjiharissi⁴, Maria Papaioannou^{1,6}, Heather Harrington⁶, Helen Doolittle¹,
Evangelos Terpos^{1,7}, Meletios Dimopoulos⁷, Saad Abdalla^{1,2}, Helen Yarranton⁸, Kikkeri
Naresh^{1,9}, Letizia Foroni^{1,2}, Alistair Reid^{1,2}, Amin Rahemtulla^{1,2}, Michael Stumpf⁶, Irene
Roberts^{1,2}, Anastasios Karadimitris^{1,2}

¹Centre for Haematology, Department of Medicine, Imperial College London, London, UK

²Department of Haematology, Hammersmith Hospital, Imperial College Healthcare NHS Trust, London, UK

³Department of Cell and Developmental Biology, University College London, UK

⁴Department of Haematology, Theageneion Hospital, Thessaloniki, Greece

⁵AHEPA Hospital, Aristoteleion University Medical School, Thessaloniki, Greece

⁶Centre for Bioinformatics and Institute of Mathematical Sciences, Imperial College London, UK

⁷Department of Clinical Therapeutics, University of Athens School of Medicine, Athens, Greece

⁸Department of Haematology, Chelsea and Westminster Hospital NHS Trust, London, UK

⁹Department of Histopathology, Hammersmith Hospital, Imperial College Healthcare NHS Trust, London, UK

Running Title: Myeloma-propagating cells and drug resistance

Text word count: 4941

Abstract word count: 198

Number of figures and Tables: 6 Figures

Number of references: 49

Correspondence: Anastasios Karadimitris

Centre for Haematology, Department of Medicine

Imperial College London

Hammersmith Hospital

Du Cane Road, London W12 0NN, UK

Tel: +44(0) 208 383 8438

Fax: +44(0) 20 3313 8223

e-mail: a.karadimitris@imperial.ac.uk

ABSTRACT

The phenotype and function of cells enriched in tumor-propagating activity and their relationship to the phenotypic architecture in multiple myeloma (MM) are controversial. Here, in a cohort of 30 patients we show that MM comprises four hierarchically organised, clonally-related sub-populations which, although phenotypically distinct, share the same oncogenic chromosomal abnormalities as well as immunoglobulin heavy chain complementarity region 3 area sequence. Assessed in xenograft assays, myeloma-propagating activity is the exclusive property of a population characterized by its ability for bi-directional transition between the dominant CD19-CD138+ plasma cell (PC) and a low frequency CD19-CD138- subpopulation (termed Pre-PC); in addition, Pre-PC are more quiescent and unlike PC, are primarily localized at extramedullary niches. As shown by gene expression profiling, compared to PC, Pre-PC are enriched in epigenetic regulators, suggesting that epigenetic plasticity underpins the phenotypic diversification of myeloma-propagating cells. Prospective assessment in paired, pre- and post-treatment bone marrow samples shows that Pre-PC are up to 300-fold more drug-resistant than PC. Thus, clinical drug resistance in MM is linked to reversible, bi-directional phenotypic transition of myeloma-propagating cells. These novel biological insights have important clinical implications in relation to assessment of minimal residual disease and development of alternative therapeutic strategies in MM.

INTRODUCTION

Multiple myeloma (MM) is an incurable plasma cell (PC) malignancy of the bone marrow (BM). Although acquired genetic events and the tumor microenvironment are well established regulators of myeloma cell survival and proliferation pathways, the identity and functional properties of the myeloma-propagating cells have been a matter of controversy^{1,2}.

The terminal differentiation of normal mature B lymphocytes to immunoglobulin (Ig)-secreting PC entails conversion of antigen-naïve to antigen-experienced B cells in the germinal centre of secondary lymphoid organs and their subsequent differentiation to either memory B cells or PC^{3,4}. Each stage of B cell differentiation can be defined by surface markers with naïve and memory B cells expressing CD19 and terminally differentiated normal and malignant PC, but not B cells, expressing CD138 (Syndecan-1)^{5,6}.

Given this linear B cell lineage developmental process, it was suggested that myeloma cell growth is sustained by a minority of cells more immature than the PC. This hypothesis is supported by the presence of CD19+CD138- clonotypic B cells [i.e. cells sharing the same Ig heavy chain (IgH) complementarity region 3 (CDR3) sequence with the myeloma PC] in peripheral blood (PB) and BM of patients with MM⁷⁻¹⁰. Indeed, since CD138- but not CD138+ PC were found to lead to myeloma engraftment in NOD/SCID mice it was proposed that CD138- cells were the principal myeloma-propagating or “myeloma stem” cells¹¹⁻¹⁴. Earlier studies though, using a huSCID mouse model, had concluded that mature PC (defined as CD38hiCD45-), and not the CD19+ B cell fraction, contained the entire myeloma-propagating activity¹⁵, while more recently, CD19-CD138- as well as CD138+ cells engrafted SCID-rab mice with myeloma¹⁶. Whether these discrepancies result from different animal models and phenotypic definitions of PC is not clear. Here, through a detailed phenotypic and genetic analysis of primary human myeloma cells and a prospective, dynamic ex vivo and in vivo study of the constituents of the myeloma cellular architecture we show that a

phenotypic and functional inter-convertible state between CD138+ and CD138- cells underpins myeloma-propagating activity and clinical drug resistance.

METHODS

Patient and normal donor bone marrow and peripheral blood samples

Patient bone marrow (BM) and peripheral blood (PB) samples were obtained after written informed consent and appropriate institutional ethics committee approval. Patient characteristics are shown in **Suppl Table 1**. Diagnosis, remission and relapse of MM were defined according to previously described criteria¹⁷. Normal BM samples were surplus material from cryopreserved bone marrow harvests, collected from healthy sibling adult donors, for use in allogeneic transplantation. Cells were collected and stored in the John Goldman Centre for Cellular Therapy at the Hammersmith Hospital, under JACIE-approved procedures and released with donor's written informed consent.

IgH CDR3 characterization of the myeloma clone and patient-specific IgH CDR3 qPCR for myeloma clonotypic cells

The IgH CDR3 characterization of the myeloma clone was performed as previously described¹⁸. A customised genomic DNA qPCR assay was used for detection and quantification of clonotypic cells (**Suppl Fig 1C**). For this purpose, patient-specific IgH CDR3 forward primer was designed in the D-N2-J_H area. IgH hydrolysis probes (TaqMan®) labelled with FAM in 5'-end and with TAMRA in the 3'-end were complementary to the 3'-end of the J_H exon, as previously published¹⁹. The reverse primer for qPCR was designed complementary to the intron downstream the J_H gene segment. Unlike other B cell malignancies, we found that in MM this intronic area is usually heavily affected by somatic hypermutation. Therefore, this intronic area was amplified in each case with a PCR using the patient specific IgH CDR3 forward primer and a J_H reverse primer complementary to the downstream J_H gene. The PCR product was characterized by nucleotide sequencing and a patient specific reverse primer was designed to improve the efficiency and specificity of

qPCR (**Suppl Fig 1D**). In selected cases, a patient-specific probe had to be designed for the same reasons. qPCR sensitivity was tested using serial dilutions of patient CD138+ cell gDNA into gDNA extracted from a pool (n=10) of normal donor B cells. The $\Delta\Delta Cq$ method was used for the relative quantitation of the myeloma clonotypic cells within the flow-sorted cell populations. The reference gene used was albumin (see also Supplementary Data).

Flow-cytometry analysis and cell-sorting

BM cells and PBMC were prepared in single cell suspension in PBS plus 0.5% BSA solution. Non-specific staining was reduced using a Fc blocking reagent (Myltenyi Biotec) and 4',6-diamidino-2-phenylindole (DAPI) was used for dead cell exclusion. Doublet cells were excluded based on FSC-W/FSC-A values. We used 12-colour flow cytometry for analysis in a BD LSRFortessa analyser and 10-colour staining for cell sorting in a BD FACSAria II cell sorter (both from BD Bioscience). The monoclonal antibodies used are listed in the Supplementary Data file. For cell cycle analysis, cells were first stained for surface markers followed by fixation for 30mins, using a fixation buffer from eBiosciences. Cells were then incubated for 20min in DAPI staining solution (DAPI 1 μ g/ml, Triton-X 0.1%). A 355nm UV laser in a BD LSRFortessa analyser was used for DAPI excitation. For Rhodamine 123 dye exclusion, cells were first stained for surface markers and then incubated in alphaMEM culture medium plus 12.5 μ M Rhodamine 123 for 10mins. Cells were then washed and placed in 37°C for 45mins before analysis. Data were analysed using the FlowJo software by Tree Star Inc., Ashland, OR.

Xenograft assays

NOD.Cg-Prkdc^{scid} Il2rg^{tm1Wjl}/SzJ (NSG) mice were obtained from Dr Paresh Vyas, Weatherall Institute of Molecular Medicine, University of Oxford, UK. All animal experiments were conducted in accordance to Animals (Scientific Procedures) Act 1986 and under a UK Government Home Office approved project licence.

NSG mice aged 9-13 weeks were first sublethally irradiated (200cGy) and cells were injected within the next 4 to 24 hours. The isolation strategy of clonotypic cells from total BM was modified, aiming to minimize exposure of transplanted cells to surface antibody labelling, especially anti-CD38. This approach was adopted to avoid opsonisation and thus reduced engraftment rates as previously reported²⁰.

CD138+ PC were first isolated from total BM with CD138+ immunomagnetic bead selection, followed by flow-sorting of the CD138^{hi} cells to high purity (~100%, **Figure 4A**). Pre-PC were negatively enriched by flow-sorting of the CD19-CD138-CD2-CD3-CD14-CD16-CD34-CD45-Glycophorin A- BM cells. Clonotypic B cells were flow-sorted using a CD19+CD138- gate. Cells were collected in PBS and immediately injected in doses up to 1.5×10^6 cells per animal (**Suppl Table 4**). In all cases, tail vein-injected cells were tested with IgH CDR3 qPCR to confirm the presence and quantify the dose of clonotypic cells given (shown in **Suppl Table 4**). Mice were followed up for a minimum period of 24 weeks. Single cell suspensions were prepared from the murine BM, liver and spleen and analysed with flow-cytometry. Human cells were identified as mCD45.1-hCD59+ and further tested for expression of CD138, CD38, CD56, CD19, CD20, CD200, CD319 and CD27 antigens. Engrafted cells were quantified as percentage of the mCD45.1+ murine hematopoietic cells. Additionally, engraftment of human cells was confirmed with IgH CDR3 qPCR, showing that the human cells found in the murine tissues were always 100% clonotypic.

Gene expression profiling

Total RNA was extracted from flow-sorted (purity >99%) PC and Pre-PC using the RNeasy Plus Micro kit (Qiagen). In all cases (n=9, **Suppl Table 5**) cells were isolated from fresh BM aspirates taken at diagnosis (n=6) or at relapse (n=3). Extracted RNA was quantified using the Qubit® Fluorometer (Invitrogen). RNA purity and integrity was confirmed in an Agilent 2100 Bioanalyser with RNA Pico Chips. Because Pre-PC is a low frequency population, we used the Ovation® Pico WTA Systems V2 from NuGEN Technologies to efficiently produce amplified cDNA for microarrays starting from a 15ng total RNA input. Amplified cDNA was

then fragmented and labelled using the Encore™ Biotin Module (NuGEN Technologies) and hybridised on Human Gene ST1.0 Arrays (Affymetrix) at a final concentration 23ng/μl in the hybridization mix on a GeneChip Fluidics Station 450. The arrays were scanned in a GeneChip® Scanner 3000 7G with autoloader.

Arrays were normalised using RMA and then non-specific filtering applied to remove probes with low variance across samples. Hierarchical clustering and heat map generation were performed using Partek on the 1000 probes showing the greatest log fold change. Differential expression analysis was applied in R/Bioconductor using the limma package with empirical Bayes correction. Principal component analysis was applied on the 1509 genes showing differential expression ($p < 0.05$) with the first principal component (PC1) clearly separating the Pre-PC-PC samples cell types. To enrich the set of genes for gene ontology (GO) term enrichment analysis, a cut on the (absolute) loadings on PC1 of 0.02 was applied giving 1094 genes for analysis. GO term enrichment was performed using DAVID with the total set of genes on the Affymetrix HG ST 1.0 as the background. P-values represent a Benjamini-Hochberg corrected modified Fisher's exact test.

Statistics

The Mann-Whitney and Wilcoxon sign rank tests were used for group comparisons. Statistical analysis was performed with the SPSS statistics v17.0 software.

Modeling and relevant statistical methods, cytology, immunohistochemistry and FISH are described in Supplemental Data.

RESULTS

Cell of origin, phenotypic diversity and genetic characterization of the myeloma cellular architecture

The presence of low frequency PB and BM clonotypic CD19+ B cells⁷⁻¹⁰ suggests that the cell of origin in MM is a CD19+ B lineage cell. To further address this, we analysed in purified myeloma PC the length of the class switch recombination (CSR) S μ - γ fusion fragment, a unique molecular event that defines transition from naïve to memory B cells²¹. Using long template PCR, as previously reported²², we found a single band in all 10 cases studied (**Suppl Fig 1A & B**) suggesting that tumor-propagating cells in MM originate from a post-CSR, germinal centre-experienced B cell.

Next, we established the complete phenotypic spectrum and quantified the frequency of B cell lineage clonotypic cells. Using a rigorous methodology combining flow-sorting of populations of interest with a highly sensitive clonotypic genomic qPCR assay specific for the patient-unique IgH CDR3 sequence (**Suppl Fig 1C-F**), we identified clonotypic CD19+ cells in both the BM and PB of patients at diagnosis, remission and relapse (**Figure 1 and Suppl Figure 1G**). In line with CSR analysis, we found that the clonotypic architecture of MM does not include naïve (CD19+IgD+) or immature (CD19+IgD-CD10+) B cells (**Figure 1A and Suppl Fig 1G**). Instead, it consists of a) mature CD19+ B cells (**Figure 1A**) comprising resting memory B cells (CD19+CD10-IgD-CD27+/-CD38-) and plasmablasts (PBL: CD19+CD10-IgD-CD38hiCD319+CD138-; **Figure 1A**) and b) CD19-CD200+CD319+CD56+ cells comprising CD138+ and CD138low PC and a previously incompletely characterised, low frequency (~3 % of all clonotypic cells) CD19-CD138-CD200+CD45-CD319+CD56+ population we termed Pre-PC (**Figure 1B and Suppl Fig 1H**). Quantitation of the clonotypic subpopulations in the BM of 30 patients with MM (**Suppl Table 1**) showed that the frequency of clonotypic cell subsets, from CD19+ cells to CD19-CD138+ PC, increases in a near logarithmic manner (**Fig 1C & E**). Unlike in BM, Pre-PC but not PC were identified in the peripheral blood (PB) of the majority of patients (**Figure 1D &**

F). In line with CD138 expression heterogeneity, CD138^{low} and CD138⁻ cells could also be identified by BM immunohistochemistry (**Suppl Figure 1I & J**). Notably, Pre-PC and PC from MM patients were morphologically distinct from each other: Pre-PC, in contrast to the large size and the prominent Golgi apparatus of PC, were significantly smaller with little or no visible Golgi and resembled small lymphocytes (**Figure 1G**).

Genetic characterization of the clonotypic hierarchy by fluorescent in situ hybridization (FISH) confirmed the presence of oncogenic cytogenetic abnormalities [such as t(11;14), t(4;14) and del13^{23, 24}] in clonotypic CD19⁺ cells as well as in PC and Pre-PC of the same patient showing that these cells are part of the same malignant clone as the CD138⁺ PC (**Figure 1H and Suppl Fig 1K & L**). Together these data show that the clonotypic architecture in MM is phenotypically more diverse than previously appreciated and bears the typical MM oncogenic genetic hallmarks.

Normal counterpart of Pre-PC in peripheral blood and bone marrow

Previous studies demonstrated the presence of circulating CD19⁺ PBL and PC in the PB of healthy individuals^{6,25}. These cells show strong expression of CD27 and CD38 (i.e., CD19⁺CD38^{hi}CD27^{hi}). However, it is unclear whether a normal counterpart of circulating Pre-PC, i.e., CD19⁻ B lineage cells with the CD38^{hi}CD27^{hi}CD319⁺CD138⁻ phenotype exists. To address this, we performed immunophenotypic analysis of PB samples from 15 healthy donors (**Figure 2A & B**). As previously described^{6,25}, within the population that expresses cytoplasmic Ig light chains (LC) and therefore comprises bone fide B lineage cells, we identified CD19⁺CD38^{hi}CD27^{hi}CD319⁺CD138⁻ PBL and CD138⁺ PC. In addition, we identified a CD19⁻cytoplasmic Ig LC⁺ population which was enriched in CD38^{hi}CD27^{hi}CD319⁺ cells. The majority of these cells CD19⁻CD38^{hi}CD27^{hi}CD319⁺ cells express CD138 and are therefore PC while a smaller proportion are CD138⁻ i.e., correspond to the myeloma Pre-PC phenotype (**Figure 2A & B**).

To further investigate the phenotypic relationship of the myeloma clonotypic architecture with that of the normal late B cell differentiation program, we applied a similar immunophenotypic strategy in normal BM samples.

In line with previous work ^{6;25}, we found that PC in normal BM are CD38hiCD27hiCD138+ cells that may or may not express CD19, while PBL are identified as CD19+CD38hiCD27hiCD138- cells (**Figure 2C**). In addition, in all 5 BM samples tested we identified a novel CD19-CD27hiCD38hiCD138- population that by immunophenotypic criteria corresponds to myeloma Pre-PC (**Figure 2C**). All 4 populations, PBL, Pre-PC and CD19+ or CD19- PC, as compared to memory and naïve B cells, displayed strong expression of surface CD319 and cytoplasmic Ig LC (**Figure 2D**). Interestingly, both BM and PB Pre-PC, as assessed by forward scatter criteria, are smaller than PC (**Figure 2B & D**). Therefore, PB and BM pre-PC are a feature of normal late B cell architecture as well as of myeloma.

Taken together, these data suggest that clonotypic cells in myeloma are organized in a hierarchy that mirrors, at least in part, that of normal late B cell development.

Mathematical modeling of growth and differentiation of myeloma clonotypic cells

Having delineated its phenotypic complexity, we tested directions of phenotypic transitions within the myeloma BM hierarchy by developing dynamic mathematical models (see **Suppl Methods** and **Suppl Tables 2 & 3** for more details) and fitting them to the observed frequencies of CD19+ cells, Pre-PC, CD138low PC and CD138+ PC using maximum likelihood²⁶. Our null model assumed a linear transition from CD19+ cells to PC via Pre-PC and CD138low cell types. Using the likelihood ratio test we examined the hypothesis of additional subset transitions. We found that while each of the Pre-PC→CD19+ cell, CD138lowPC→CD19+ cell, PC→CD19+ cell transitions were not supported in the analysis ($p=0.999$), a PC→Pre-PC transition could be readily identified ($p=0.031$; **Figure 3A and Suppl Figure 2**). We further investigated the PC→Pre-PC transition by adopting a Bayesian approach and using an MCMC algorithm²⁷, calculated the marginal likelihood under the null model and the model including the PC→Pre-PC transition (**Figure 3B**). We obtained a

median Bayes Factor of 5.06 thus providing strong evidence for the existence of this transition²⁸ suggesting that Pre-PC and PC might exist in an inter-convertible state.

Tumor-propagating activity of myeloma clonotypic subsets

To directly test the predictions of the modeling analysis and the functional relationship of the clonotypic fractions in vivo, we adoptively transferred either highly purified CD19+ cells (i.e., a mixture of resting memory B cells and PBL), PC or Pre-PC from 8 MM patients into sub-lethally irradiated NOD/SCID/IL-2R $\gamma^{-/-}$ (NSG) mice and followed their engraftment for up to 34 weeks (**Suppl Table 4**).

As assessed by flow-cytometry combined with clonotypic qPCR and immunohistochemistry, mice transplanted with highly purified CD138hi PC displayed BM engraftment in 75% (9/12) of cases (**Figure 4A and Suppl Table 4**), showing that contrary to recent data¹¹⁻¹³, CD138+ PC can engraft immunodeficient mice and therefore are myeloma-propagating, a finding supported by their ability to engraft in secondary transplants (**Suppl Figure 3 and Suppl Table 4**). In line with the modeling analysis prediction of a PC→Pre-PC transition, both Pre-PC and CD138+/low PC were identified in BM of mice receiving CD138hi PC, at frequencies similar to those found in patients' corresponding BM samples (**Figure 4A&B**). Engrafted PC and Pre-PC had the same distinct morphological (**Figure 4C**) and cell cycle status features (**Figure 4D**) as in the patient BM (see below and **Figure 6D**), i.e., pre-PC were smaller and more quiescent cells, thus recapitulating the original, clonotypic Pre-PC - CD138low - PC hierarchy observed in the patient BM. However, as also predicted by the modeling analysis, CD19+ human cells were never detected (data not shown) in the BM of these mice.

We also found clonotypic cells in the spleen and liver of mice transplanted with CD138hi PC, although at an overall lower frequency than in BM (**Suppl Table 4**). Notably, unlike the BM where CD138+ PC comprised the majority of clonotypic cells, the spleen and liver contained predominantly Pre-PC and CD138low myeloma cells rather than CD138+ PC (**Figure 4A & B**). These data support the important role played by the microenvironment in modulating the

behavior of MM clonotypic cells and suggest that preferential microenvironmental localization as well as phenotypic differences distinguish Pre-PC from PC.

To formally test in vivo the Pre-PC → PC transition, negatively enriched (to avoid anti-CD38 mAb-mediated cell opsonization²⁰) Pre-PC were transferred into NSG mice. Despite a lower engraftment rate (25%, 4/16 mice; **Suppl Table 4**), which is likely to reflect the lower numbers of cells available compared to PC, the pattern of CD138 expression in BM was similar to that generated by CD138hi PC, i.e., predominance of CD138+ PC over Pre-PC (**Figure 4E**). Finally, as previously reported^{16,15} none of the mice (0/10) transplanted with CD19+ cells showed evidence of engraftment (**Suppl Fig 4**) supporting lack of myeloma-propagating activity in CD19+ clonotypic cells.

Together these data indicate that within the myeloma phenotypic hierarchy, myeloma-propagating activity is the exclusive property of a population which can assume two inter-convertible phenotypic states distinguished by their expression of CD138. Interestingly, the preferential localization of cells with low or no expression of CD138 in the liver and spleen of engrafted animals, and their preferential presence in PB of patients, suggests the existence of extramedullary 'MM niches'. In line with extramedullary 'MM niches' in humans, prospective analysis of several paired BM-PB samples in patient P12 (**Suppl Table 1**) over a period of 38 months showed in two consecutive time points the presence of circulating Pre-PC and clonotypic CD19+ cells while the patient was in complete clinical remission¹⁷ and in molecular remission in the BM (**Figure 4F**).

Global mRNA expression profiling of Pre-PC - PC

To gain insights into the molecular mechanisms underpinning the reversible, bi-directional Pre-PC - PC transition we subjected highly purified (>99%) Pre-PC - PC pairs from 9 patients (**Suppl Table 5**) to global mRNA expression profiling. Hierarchical clustering of the 1000 genes with the highest fold change in mRNA expression between the two cell types revealed distinct clusters of gene expression separating PC from Pre-PC in 7 samples, while the other 2 samples formed a different distinct pattern (**Figure 5A**). Further analysis focused

on the 7 samples sharing the same hierarchical clustering pattern (**Figure 5B**) identifying 1509 differentially expressed genes at $p < 0.05$. A principal component analysis (PCA) of these genes showed clear separation of PC and Pre-PC along the first principal component in all 7 pairs ($p = 4 \times 10^{-6}$; **Figure 5C and Suppl Figure 4**). To reduce our gene set for pathway analysis and enrich for those genes involved in separating PC and Pre-PC, a threshold on the loading of the first principal component was applied resulting in 1094 genes. This set was highly enriched ($p \ll 0.01$) in Pre-PC for genes involved in chromatin modification, chromatin and chromosome organization (**Figure 5D**). Upon functional annotation clustering using DAVID (**Suppl Table 6**), a graph-based algorithm²⁹, the highest scoring cluster contained several chromatin regulators, including histone methyl-transferases (belonging to the Polycomb repressive complex 2 or Trithorax MLL activating complex) and demethylases, histone acetyl-transferases and de-acetylases as well as several members of SWI/SNF chromatin remodeling complex (**Figure 5E and Suppl Table 7**).

Also enriched in the highest scoring cluster were TLK1 and TLK2, two genes implicated in double-strand DNA repair and linked to tumor radio- and chemo-resistance³⁰⁻³³.

Taken together, these findings suggest an important role of 'epigenetic plasticity' determining the process of bi-directional transition of myeloma-propagating cells.

Pre-PC and clinical drug resistance

Since reduction or loss of CD138 expression was previously associated with increased chemoresistance of a myeloma cell line in vitro³⁴, we addressed whether Pre-PC - PC transition is linked to differential treatment responses in primary MM cells in vivo. For this purpose, we first compared the frequency of clonotypic CD19+ cells, Pre-PC and PC in patients at diagnosis with those in remission following treatment that included chemotherapy, the proteasome inhibitor bortezomib and autologous hematopoietic stem cell transplantation (**Suppl Table 1**). As expected, the PC frequency in the BM from diagnosis to remission was significantly lower ($p = 0.013$; **Figure 6A**). However, consistent with clinical drug resistance,

the frequency of BM CD19+ clonotypic cells and Pre-PC remained unchanged ($p>0.05$; **Figure 6A**).

To further investigate the resistance of Pre-PC to treatment, we carried out a prospective quantitative assessment of BM clonotypic cells in paired pre-treatment and post-treatment clinical remission samples from 8 MM patients. Consistent with clinical drug resistance, in all 8 patients, a significantly higher proportion of Pre-PC than PC persisted post-treatment, with an overall 10.3-fold smaller reduction (range 4.4-332; $p=0.008$) in the frequency of Pre-PC as compared to PC (**Figure 6B & C**). Although Pre-PC were more quiescent than PC as revealed by the significantly ($p=0.01$) higher proportion of Pre-PC in S phase of the cell cycle (**Figure 6D**), a property also consistent with drug resistance, both Pre-PC and PC excluded vital dye equally efficiently and lacked surface expression of the drug efflux proteins ABCB1 (P-glycoprotein) and ABCG2³⁵ (**Figure 6E**) suggesting that their differential response to treatment does not involve a drug efflux mediated-process commonly implicated in tumor chemo-resistance.

Taken together, these data show that both PC and Pre-PC fractions harbor myeloma-propagating activity and represent two dynamic and inter-convertible states of the same clonal population displaying differential response to treatment and preference for extramedullary niches.

DISCUSSION

In this study, we investigated myeloma-propagating activity based on the most comprehensive dissection of the phenotypic diversity in myeloma to date. While previous studies suggested the presence of CD19+CD138- clonotypic cells as well as the dominant CD19-CD138+ PC, we show that the myeloma cellular architecture comprises at least 4 distinct populations. The data that emerged from the large cohort of MM patients we studied, strongly suggests a hierarchical arrangement of these populations, mirroring that of normal B cells, i.e., with clonotypic memory B cells followed by CD19+ PBL at the apex of the hierarchy and the CD19-CD138+ PC as the most mature cellular population. The CD19-CD38hiCD319+CD138- immunophenotype of Pre-PC, a population only incompletely studied in myeloma, suggested that within this hierarchy, Pre-PC are placed between PBL and PC. This is further supported by a) high expression in Pre-PC of CD319, a SLAM family receptor highly expressed in normal and malignant PC³⁶, b) identification both in BM and PB of normal individuals of a population with exactly the same phenotype as myeloma Pre-PC, i.e., CD19-CD38hiCD319+CD138- cells and c) the ability of Pre-PC to generate PC but not PBL in the xenograft assays.

As shown in Figure 2 and previously reported²⁵, PBL, i.e., CD38hiCD27hiCD319+CD138- cells that express CD19 comprise a sizeable fraction of normal late B cell development. PBL are considered to represent differentiating, Ig-secreting cells migrating from secondary lymphoid organs to the BM where they complete their maturation to CD38hiCD27hiCD319+CD138+ PC⁶, with the majority of normal BM PC retaining expression of CD19. However, in myeloma, CD19+CD38hiCD319+CD138- clonotypic, PBL-like cells, when detected, comprised only a small fraction of the clonotypic population (data not shown) while, as previously reported³⁷, the dominant myeloma PC were CD19- in all cases, suggesting a specific propensity of CD19- but not of CD19+ late B cell lineage cells to myelomatous transformation.

In principle, Pre-PC in myeloma could be generated through forward differentiation of clonotypic CD19+ B cells or by reverse differentiation of mature CD138+ PC. The detailed and precise phenotypic and molecular data accrued from 30 patients allowed the development of a mathematical model that was constructed assuming a forward CD19+→Pre-PC→CD138low→PC differentiation potential and was used to ask whether reverse differentiation programs were possible. It clearly showed that only a PC→Pre-PC transition was possible, suggesting a distinct role of Pre-PC - PC bidirectional transition in the biology of myeloma. Xenograft assays, as well as confirming this prediction, they also showed that Pre-PC - PC bidirectional transition is a phenomenon observed irrespective of the primary oncogenic genetic events or clinical stage of disease (**Suppl Table 1 & 4**).

Unlike myeloma PC and Pre-PC, clonotypic primary CD19+ B cells (i.e., memory B cells and PBL) failed to engraft. This may reflect either insufficient numbers of clonotypic cells injected (i.e. a 5-fold smaller dose of pre-PC than PC were transferred into NSG mice; **Suppl Table 4**), dependence of these cells on external cues that are not provided by the microenvironment in NSG mice or lack of myeloma-propagating activity of CD19+ clonotypic cells as previously reported¹⁵.

Taken together, our in vivo experiments clearly demonstrated that the myeloma-propagating activity is a property shared by both CD19-CD138- Pre-PC and CD19-CD138+ PC but it does not appear to include CD19+CD138- clonotypic B cells, thus resolving the current uncertainty whether CD138+ versus CD138- cells are enriched in tumor-propagating activity¹.

Pre-PC not only resemble small lymphocytes and are more quiescent than PC, they are also molecularly distinct to PC as shown by mRNA expression profiling and principal component analysis. The molecular signature of Pre-PC comprises epigenetic regulators enriched in critical components of the Polycomb repressive complex, MLL transcriptional activating complex and the chromatin remodeler SWI/SNF. Polycomb and MLL are multi-protein complexes that in concert operate to impose a bivalent chromatin status, i.e., co-existence of positive and negative histone methylation marks in the promoters and enhancers of

developmental genes and genes encoding lineage-affiliated transcription factors regulating thus the epigenetic plasticity that underpins pluripotency of germ and somatic stem cells^{38 39}. We speculate that through their higher expression in Pre-PC, these complexes may play a similar role in determining the epigenetic plasticity that controls the bidirectional Pre-PC - PC transition (**Figure 6F**).

Non-genetic, including epigenetic, clonal diversification has previously been predicted on theoretical grounds^{40;41} and experimentally addressed in multipotent hematopoietic progenitor⁴² and cancer cell lines⁴³ *in vitro*. The same process was shown to underlie the transient and reversible drug-tolerant states of a small minority of cells (termed drug tolerant persisters – DTP) in a variety of human cell lines *in vitro*⁴³. Our finding that the low frequency, phenotypically and molecularly distinct Pre-PC are significantly less sensitive to anti-myeloma treatment than PC, provides strong support for the importance of non-genetic mechanisms in instructing clinical drug resistance also *in vivo* in primary tumors; the lack of a drug efflux mechanism associated with clinical drug resistance in myeloma is another feature that Pre-PC share with DTP⁴³. Interestingly, higher expression of the histone lysine demethylase KDM5A was linked to the emergence of DTP⁴³ and our gene expression profiling shows that Pre-PC are also enriched in a number of histone lysine demethylases. Enrichment in expression of TLK1 and TLK2, two highly homologous Ser/Thr kinases, involved in nucleosome remodeling and double strand DNA repair through phosphorylation of Rad9 and Asf1 respectively^{33;44}, could constitute another mechanism of Pre-PC drug resistance. Indeed, over-expression of TLK1 has been associated with increased radio- and chemo-resistance in cancer cell lines³⁰⁻³².

Nevertheless, it is likely, if not certain, that irreversible genetic, mutational mechanisms would eventually also instruct myeloma-propagating activity as well as drug resistance. In fact, it is predicted^{40;41} that non-mutational diversification may promote and co-operate with mutational mechanisms leading to clonal evolution. Finally, it should be noted that CD138 mRNA was not differentially expressed between Pre-PC and PC (data not shown) suggesting that its downregulation in Pre-PC is mediated primarily through post-

transcriptional mechanisms, likely, by its cleavage at the cell surface⁴⁵. Whether down-regulation of CD138 expression in itself is necessary or it is just a marker for the Pre-PC - PC transition remains to be determined.

The observation that the PC↔Pre-PC equilibrium is subject to microenvironmental constraints, with the CD138+ status predominant in BM and the CD138- status predominant in the spleen, liver and possibly other anatomical sites of the engrafted animals, provides another example of the close relationship between myeloma and microenvironment. Consistent with previous observations in tumor models showing the ability of the microenvironment to impart de novo drug resistance and shape phenotypic diversity of tumor cells through non-genetic mechanisms⁴⁶, the data presented here suggest that extramedullary locations function as sanctuaries of drug resistance and relapse in myeloma. This is further highlighted by a) patient P12 in whom Pre-PC but not PC persisted in PB despite complete clinical and molecular remission in the BM in two consecutive time points in the course of the disease and b) the clinical observation that in up to 35% of patients with MM, following high dose chemoradiotherapy and autologous or allogeneic stem cell transplantation, relapse can take place in extramedullary sites without evidence of concurrent BM disease^{47;48}.

From a clinical perspective, our findings suggest that current methods of assessing minimal residual disease relying on the identification of CD138+ cells in the BM³⁷ should be re-evaluated to include CD138- clonotypic cells in blood as well as BM. Moreover, use of mAb for therapeutic targeting of CD138⁴⁹ might favor survival of inherently drug-resistant, myeloma-propagating cells and current and future therapeutic strategies should aim at effectively targeting all clonotypic myeloma fractions. Finally, delineation of the precise role of the epigenetic regulators such as Polycomb and MLL in the Pre-PC - PC transition will offer opportunities for development of novel epigenetic therapies in MM.

Acknowledgments

This work was supported by Leukaemia and Lymphoma Research, Leuka and the NIHR Biomedical Research Centre.

Author Contributions

AC: designed and performed research, analysed data, wrote the paper; CPB: performed mathematical modeling, analysed data, wrote the paper; HH, MS: performed mathematical modeling, analysed data; GC, PCM, VM, AR, HD: perform researched, analysed data; EH, MP, ET, MD, SA, HY, AR: contributed patient samples and information, contributed to manuscript writing; KN, LF: supervised part of research, analysed data; IR: analysed data, contributed to the writing of paper, supervised research; AK: designed and supervised research, analysed data, wrote the paper

Conflict of Interest Disclosures

The Authors have no relevant conflict of interests to declare

References

1. Anderson KC, Carrasco RD. Pathogenesis of myeloma. *Annu.Rev Pathol.* 2011;6:249-274.
2. Morgan GJ, Walker BA, Davies FE. The genetic architecture of multiple myeloma. *Nat Rev Cancer* 2012;12:335-348.
3. Oracki SA, Walker JA, Hibbs ML, Corcoran LM, Tarlinton DM. Plasma cell development and survival. *Immunol Rev* 2010;237:140-159.
4. Bernasconi NL, Traggiai E, Lanzavecchia A. Maintenance of serological memory by polyclonal activation of human memory B cells. *Science* 2002;298:2199-2202.
5. Sanz I, Wei C, Lee FE, Anolik J. Phenotypic and functional heterogeneity of human memory B cells. *Semin Immunol* 2008;20:67-82.
6. Perez-Andres M, Paiva B, Nieto WG et al. Human peripheral blood B-cell compartments: a crossroad in B-cell traffic. *Cytometry B Clin Cytom.* 2010;78 Suppl 1:S47-S60.
7. Bergsagel PL, Smith AM, Szczeppek A et al. In multiple myeloma, clonotypic B lymphocytes are detectable among CD19+ peripheral blood cells expressing CD38, CD56, and monotypic Ig light chain. *Blood* 1995;85:436-447.
8. Chen BJ, Epstein J. Circulating clonal lymphocytes in myeloma constitute a minor subpopulation of B cells. *Blood* 1996;87:1972-1976.
9. Rasmussen T, Lodahl M, Hancke S, Johnsen HE. In multiple myeloma clonotypic. *Leuk.Lymphoma* 2004;45:1413-1417.
10. Rasmussen T, Jensen L, Honore L, Andersen H, Johnsen HE. Circulating clonal cells in multiple myeloma do not express CD34 mRNA, as measured by single-cell and real-time RT-PCR assays. *Br.J Haematol.* 1999;107:818-824.
11. Huff CA, Matsui W. Multiple myeloma cancer stem cells. *J Clin.Oncol.* 2008;26:2895-2900.
12. Matsui W, Huff CA, Wang Q et al. Characterization of clonogenic multiple myeloma cells. *Blood* 2004;103:2332-2336.
13. Matsui W, Wang Q, Barber JP et al. Clonogenic multiple myeloma progenitors, stem cell properties, and drug resistance. *Cancer Res* 2008;68:190-197.
14. Peacock CD, Wang Q, Gesell GS et al. Hedgehog signaling maintains a tumor stem cell compartment in multiple myeloma. *Proc.Natl.Acad.Sci.U.S.A* 2007;104:4048-4053.
15. Yaccoby S, Epstein J. The proliferative potential of myeloma plasma cells manifest in the SCID-hu host. *Blood* 1999;94:3576-3582.
16. Hosen N, Matsuoka Y, Kishida S et al. CD138-negative clonogenic cells are plasma cells but not B cells in some multiple myeloma patients. *Leukemia* 2012; Mar 20 [Epub ahead of print]

17. Durie BG, Harousseau JL, Miguel JS et al. International uniform response criteria for multiple myeloma. *Leukemia* 2006;20:1467-1473.
18. Mortuza FY, Moreira IM, Papaioannou M et al. Immunoglobulin heavy-chain gene rearrangement in adult acute lymphoblastic leukemia reveals preferential usage of J(H)-proximal variable gene segments. *Blood* 2001;97:2716-2726.
19. Verhagen OJ, Willemse MJ, Breunis WB et al. Application of germline IGH probes in real-time quantitative PCR for the detection of minimal residual disease in acute lymphoblastic leukemia. *Leukemia* 2000;14:1426-1435.
20. Taussig DC, Miraki-Moud F, Anjos-Afonso F et al. Anti-CD38 antibody-mediated clearance of human repopulating cells masks the heterogeneity of leukemia-initiating cells. *Blood* 2008;112:568-575.
21. Stavnezer J, Guikema JE, Schrader CE. Mechanism and regulation of class switch recombination. *Annu.Rev Immunol* 2008;26:261-292.
22. Taylor BJ, Kriangkum J, Pittman JA et al. Analysis of clonotypic switch junctions reveals multiple myeloma originates from a single class switch event with ongoing mutation in the isotype-switched progeny. *Blood* 2008;112:1894-1903.
23. Fonseca R, Bergsagel PL, Drach J et al. International Myeloma Working Group molecular classification of multiple myeloma: spotlight review. *Leukemia* 2009;23:2210-2221.
24. Palumbo A, Anderson K. Multiple myeloma. *N Engl J Med* 2011;364:1046-1060.
25. Caraux A, Klein B, Paiva B et al. Circulating human B and plasma cells. Age-associated changes in counts and detailed characterization of circulating normal C. *Haematologica* 2010;95:1016-1020.
26. Cox DR, Hinkely DV. Theoretical Statistics.: Chapman and Hall/CRC; 1979.
27. Andrieu C, Djuric PM, Doucet A. Robust full Bayesian learning for radial basis networks. *Signal Processing* 2001;81:19-37.
28. Gelman A, Carlin JB, Sternberg A, Rubin DB. Bayesian Data Analysis.: Chapman and Hall/CRC; 2003.
29. Huang DW, Sherman BT, Lempicki RA. Systematic and integrative analysis of large gene lists using DAVID bioinformatics resources. *Nat.Protocols* 2008;4:44-57.
30. Takayama Y, Kokuryo T, Yokoyama Y et al. Silencing of Tousled-like kinase 1 sensitizes cholangiocarcinoma cells to cisplatin-induced apoptosis. *Cancer Letters* 2010;296:27-34.
31. Byrnes KW, DeBenedetti A, Holm NT et al. Correlation of TLK1B in Elevation and Recurrence in Doxorubicin-Treated Breast Cancer Patients with High eIF4E Overexpression. *Journal of the American College of Surgeons* 2007;204:925-933.
32. Groth A, Lukas J, Nigg EA et al. Human Tousled like kinases are targeted by an ATM- and Chk1-dependent DNA damage checkpoint. *EMBO J* 2003;22:1676-1687.

33. Sunavala-Dossabhoy G, De Benedetti A. Tousled homolog, TLK1, binds and phosphorylates Rad9; TLK1 acts as a molecular chaperone in DNA repair. *DNA Repair* 2009;8:87-102.
34. Zlei M, Egert S, Wider D et al. Characterization of in vitro growth of multiple myeloma cells. *Exp Hematol*. 2007;35:1550-1561.
35. Donnenberg VS, Donnenberg AD. Multiple drug resistance in cancer revisited: the cancer stem cell hypothesis. *J Clin Pharmacol*. 2005;45:872-877.
36. Hsi ED, Steinle R, Balasa B et al. CS1, a Potential New Therapeutic Antibody Target for the Treatment of Multiple Myeloma. *Clin Cancer Res* 2008;14:2775-2784.
37. Rawstron AC, Orfao A, Beksac M et al. Report of the European Myeloma Network on multiparametric flow cytometry in multiple myeloma and related disorders. *Haematologica* 2008;93:431-438.
38. Fisher CL, Fisher AG. Chromatin states in pluripotent, differentiated, and reprogrammed cells. *Curr Opin Genet Dev*. 2011;21:140-146.
39. Bernstein BE, Mikkelsen TS, Xie X et al. A bivalent chromatin structure marks key developmental genes in embryonic stem cells. *Cell* 2006;125:315-326.
40. Huang S, Ernberg I, Kauffman S. Cancer attractors: a systems view of tumors from a gene network dynamics and developmental perspective. *Semin Cell Dev Biol* 2009;20:869-876.
41. Huang S. Non-genetic heterogeneity of cells in development: more than just noise. *Development* 2009;136:3853-3862.
42. Chang HH, Hemberg M, Barahona M, Ingber DE, Huang S. Transcriptome-wide noise controls lineage choice in mammalian progenitor cells. *Nature* 2008;453:544-547.
43. Sharma SV, Lee DY, Li B et al. A chromatin-mediated reversible drug-tolerant state in cancer cell subpopulations. *Cell* 2010;141:69-80.
44. Canfield C, Rains J, De BA. TLK1B promotes repair of DSBs via its interaction with Rad9 and Asf1. *BMC Mol Biol* 2009;10:110.
45. Teng YH-F, Aquino RS, Park PW. Molecular functions of syndecan-1 in disease. *Matrix Biology* 2012;31:3-16.
46. Marusyk A, Almendro V, Polyak K. Intra-tumour heterogeneity: a looking glass for cancer? *Nat Rev Cancer* 2012;12:323-334.
47. Chong G, Byrnes G, Szer J, Grigg A. Extramedullary relapse after allogeneic bone marrow transplantation for haematological malignancy. *Bone Marrow Transplant*. 2000;26:1011-1015.
48. Terpos E, Rezvani K, Basu S et al. Plasmacytoma relapses in the absence of systemic progression post-high-dose therapy for multiple myeloma. *Eur J Haematol*. 2005;75:376-383.

49. Ikeda H, Hideshima T, Fulciniti M et al. The monoclonal antibody nBT062 conjugated to cytotoxic Maytansinoids has selective cytotoxicity against CD138-positive multiple myeloma cells in vitro and in vivo. *Clin Cancer Res* 2009;15:4028-4037.

FIGURE LEGENDS

Figure 1. Phenotypic and genetic characterization of the clonotypic cellular architecture in myeloma. **A.** Multi-parameter flow-cytometry gating strategy for identification and flow-sorting of CD19+ fractions (immature, naïve, memory B cells and plasmablasts - PBL) in the BM of patients with myeloma. Each of the indicated fractions was flow-sorted to high purity and subjected to patient-specific clonotypic gDNA qPCR. **B.** Top panel: Strategy for characterization of CD19- clonotypic populations. Sequential gating of patient BM CD200+CD319+ and CD45low/-CD56+ cells allows identification and flow-sorting of an almost entirely clonotypic hierarchy of CD138+ (PC), CD138low and CD138- (Pre-PC) cells. Bottom panel: overlays of the CD19- clonotypic cells (red) over the total BM cells (grey) indicates that if the traditional gating on CD138+CD38+ events was applied, it would exclude Pre-PC and CD138low cells from further analysis. **C-F.** Frequency of clonotypic fractions in BM mononuclear cells (n=30 patients; **C & E**) and peripheral blood mononuclear cells (n=21 patients; **D & F**) of patients with myeloma shown as a cohort (**C, D**) or in individual patients (**E, F**). Horizontal bars indicate median values excluding cases with undetectable clonotypic cells. **G.** Top: May-Grünwald Giemsa staining of flow-sorted Pre-PC and PC (x1000), bottom: histogram and median FSC-A values of Pre-PC and PC. **H.** Interphase FISH analysis of chromosome 13 complement showing loss of one red (13q34) and one green signal (13q14), consistent with monosomy 13 in highly purified, flow-sorted peripheral blood PBL, Pre-PC and PC from the same patient, confirmed as enriched in clonotypic cells by qPCR. Chromosome 13 ideogram and location of FISH probes are shown on the left.

Figure 2. CD19-CD138- Pre-PC are a feature of the normal late B cell development. **A.** Flow-cytometric analysis of the normal late B cell development in PB (n=15 normal donors); a representative donor sample is shown. After gating out non-B cell lineage cells, analysis of CD19+ cells, as expected, shows a polyclonal pattern of cytoplasmic Ig light chain (LC) expression, i.e. expression of κ and λ chains. PBL are identified as CD38hiCD27hiCD138-

and PC as CD38hiCD27hiCD138+ cells. For identification of Pre-PC, gating on lineage-CD19- cells reveals a small cytoplasmic Ig LC+ population which upon sequential gating is found to be enriched in CD38hiCD27hi cells (48% in the case shown); these include CD138+ PC and CD138- Pre-PC. Both CD19+ PBL/PC and CD19- Pre-PC/PC are CD319+.

B. Histograms showing cell size as assessed by FSC-A and expression levels of CD19, cytoplasmic Ig LC and CD319 in the above four populations as well as in naïve and memory B cells. Numbers next to histograms represent median intensity fluorescence (MFI) values.

C. Identification of PBL, CD19+ PC, Pre-PC and CD19- PC in BM from healthy donors; a representative of five samples is shown. Using a strategy similar to that described for PB, all four cell types were found to be CD38hiCD27hi. **D.** Histograms showing cell size and expression levels of CD19, cytoplasmic Ig LC and CD319 of BM B lineage populations.

Figure 3. Modeling analysis of differentiation and proliferation profiles of myeloma clonotypic fractions.

A. Likelihood analysis: the different cell types are represented by the grey squares and transitions between them represented by arrows (with associated rate parameters; see **Suppl Methods**). The set of black solid arrows represent the transitions in the null model that assumes linear transition from CD19+ cells to PC via Pre-PC and CD138low cell types. Each dashed arrow represents an included transition tested (i.e., Pre-PC→CD19+ cell, CD138lowPC→CD19+ cell, PC→CD19+ cell transitions) with respect to the null model using a likelihood ratio test. Black dashed lines are transitions that were not significant. The transition PC→Pre-PC (represented by the dashed red line) showed a p value of 0.031 indicating significance at the 5% level. **B.** Bayesian analysis of the transition PC→Pre-PC: to further investigate this transition an MCMC algorithm was developed to fit a fully Bayesian model. The box plot shows the marginal likelihood for the null model and for the null model including the transition PC→Pre-PC for ten runs of the MCMC algorithm with different starting values. The Bayes factor of 5.06, here calculated as the ratio of the marginal likelihoods, represents strong evidence for the inclusion of the PC→Pre-PC transition.

Figure 4. Myeloma-propagating potential of Pre-PC and PC and partial recapitulation of the clonotypic hierarchy in NSG mice. **A.** Left: Highly purified BM CD138hi myeloma PC transferred to NSG mice engraft murine BM, spleen and liver. Human cells are identified in mouse tissues by flow cytometry as hCD59+mCD45.1- (top panels). Engrafted PC recapitulate the CD19- hierarchy of the human BM (bottom panels); however, in the spleen and liver there is preferential presence of Pre-PC and CD138low cells. Right: BM H&E staining in a mouse transplanted with CD138hi PC shows myeloma cell infiltration. Immunohistochemistry (x400) for human κ/λ light chains and CD138 are also shown. In this example, myeloma PC are κ LC restricted and as expected express CD138. **B.** Cumulative data of the frequencies of PC, CD138low and Pre-PC in the BM, spleen and liver in mice receiving patient CD138hi PC. Horizontal lines represent median values. **C.** Size of BM PC and Pre-PC highly purified by flow-sorting from the BM of mice engrafted after transfer of CD138hi myeloma PC. A representative example is shown. **D.** Cell cycle analysis in multi-parameter flow cytometry of engrafted BM Pre-PC and PC. **E.** Engraftment pattern in the murine BM after transfer of Pre-PC recapitulates Pre-PC - PC duality. Pre-PC were negatively selected by flow-sorting as Lin-CD19-CD34-CD138- cells. In this example, 13.4% of the flow-sorted cells were clonotypic as assessed by qPCR and a total of 33.5×10^3 clonotypic B cells were infused. **F.** Peripheral blood and BM clonotypic cell dynamics in the timeline of treatment of a patient with MM (ASCT: autologous stem cell transplantation, Bort/Dex: bortezomib & dexamethasone) and disease status changes (MoIR: molecular remission, IF: immunofixation, CR: complete clinical remission). Blood clonotypic CD19+ cells, Pre-PC and CD138low cells but not PC are identified while the patient was in complete clinical and molecular remission in the BM at 5.6 and 11.1 months.

Figure 5. Global mRNA profile analysis of Pre-PC and PC. **A.** Hierarchical clustering of all 9 Pre-PC and PC pairs. **B.** Hierarchical clustering of the 1000 more differentially expressed genes in 7 pairs of Pre-PC- and PC. **C.** Principal component analysis on 1509

differentially expressed genes (at $p < 0.05$) in which PC and Pre-PC were clearly separated along the first principal component in all 7 pairs. **D.** Pathway analysis of genes involved in separating PC and Pre-PC. The 3 top scoring gene clusters are enriched in Pre-PC and contain genes involved in chromatin modification, chromatin organization and chromosome organization. P-values represent a Benjamini-Hochberg corrected modified Fisher's exact test. **E.** Heatmap of the genes comprising the top scoring cluster of chromatin regulators. Genes of the SWI/SNF and other remodeling complexes are shown in yellow, those of the Polycomb complex are shown in green, those of involved in histone methylation (including members of the MLL complex) and demethylation in pink and those in histone acetylation and de-acetylation in grey.

Figure 6. Drug-resistance and quiescence of Pre-PC in vivo. **A.** Frequencies of BM clonotypic cells at diagnosis (D), remission (Rem) and relapse (Rel). **B.** Frequency (top panels) and fold change (bottom panels) of clonotypic fractions in 8 patients achieving clinical remission after treatment. Top panels show absolute frequency changes in the clonotypic fractions, bottom panel shows relative changes in the frequency of the clonotypic cells. **C.** The ratio of PC/Pre-PC fold reduction (median 10.3; range 4.4 – 332; $p = 0.008$) as estimated in each patient from panel C. **D.** Cell cycle analysis after DAPI staining and multi-parameter flow cytometry of BM cells shows that a significantly lower fraction of Pre-PC than PC are in S phase. An example and cumulative data from 7 patients are shown. **E.** Left: Flow-cytometry histograms showing Rhodamine 123 dye exclusion by myeloma Pre-PC and PC as compared to PBL, naive and memory B cells. Unstained PC are shown as a negative control. PC and Pre-PC retain comparable levels of Rhodamine 123 as assessed by MFI; right: P-glycoprotein (ABCC1) and ABCG2 are not expressed in Pre-PC or PC as assessed by flow-cytometry in BM samples. Representative of 10 patient samples. **F.** A model of clonotypic hierarchy and myeloma propagating activity. Memory B cells are at the apex of the clonotypic hierarchy in MM. However, myeloma propagating activity is detected in the terminally differentiated B lineage cell that through an epigenetic, bi-directional

transition can assume the morphologically and immunophenotypically distinct states of Pre-C and PC. In most patients the equilibrium of Pre-PC \leftrightarrow PC transition favors PC. Although both are enriched in myeloma propagating activity, Pre-PC are relatively more quiescent and treatment-resistant than PC and *in vivo* are preferentially present in spleen and liver while PC are the dominant population in BM.

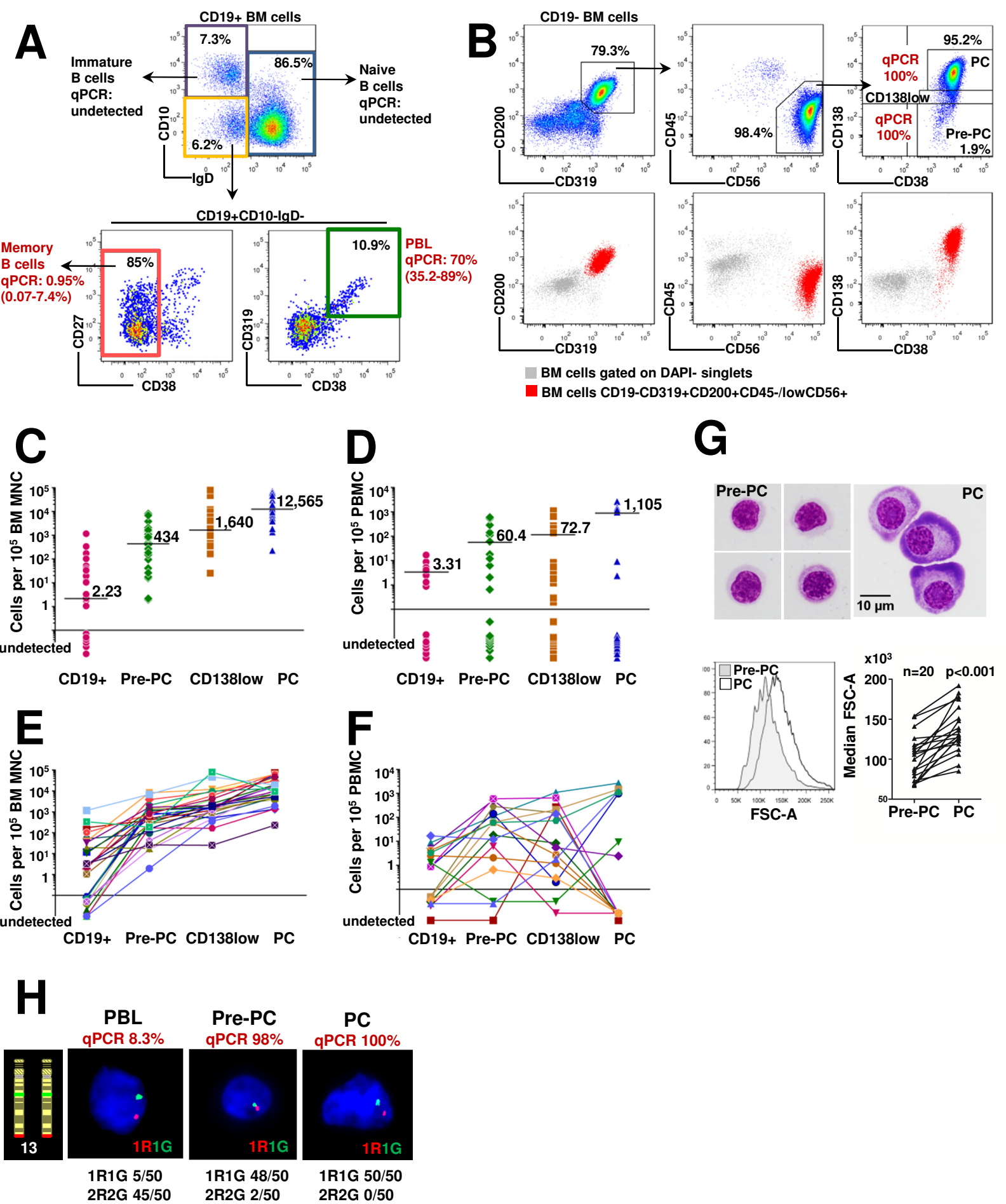
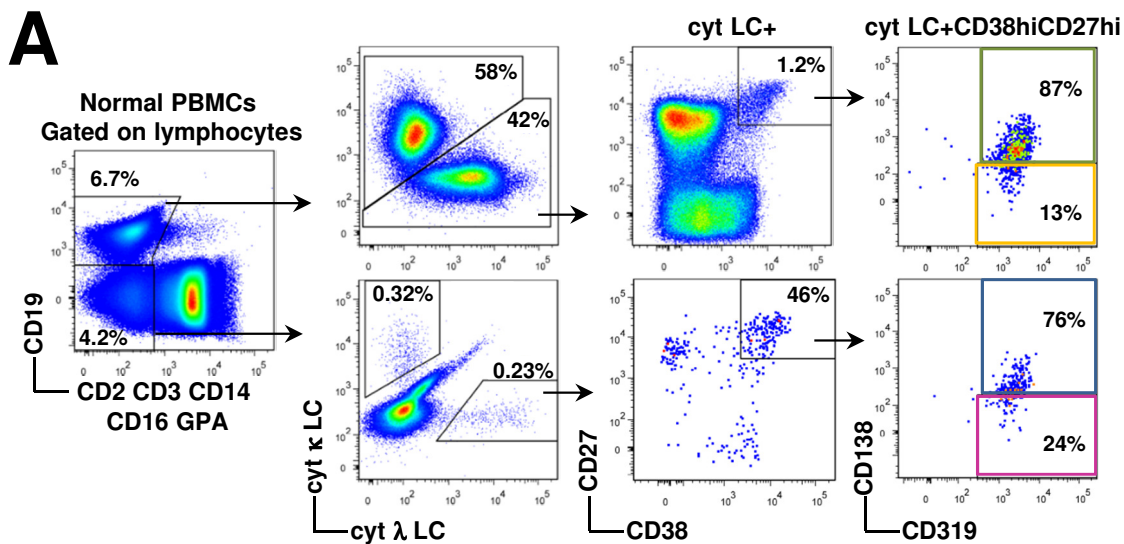
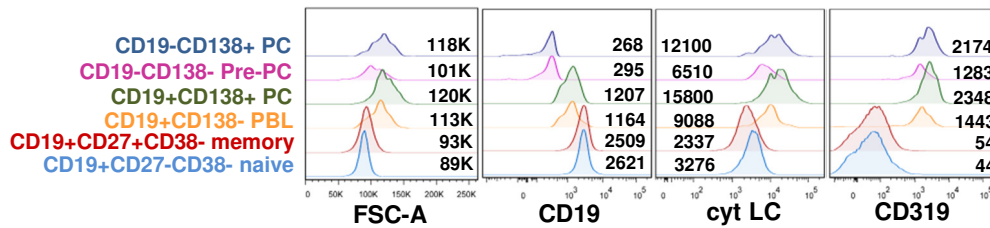


Figure 1

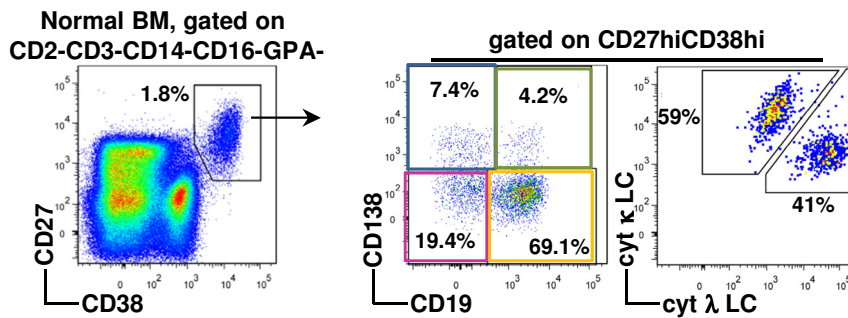
A



B



C



D

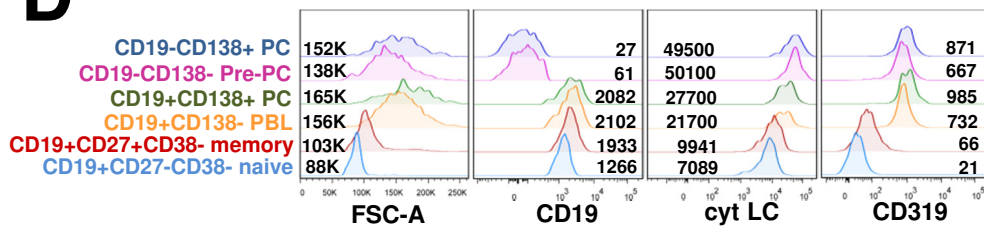
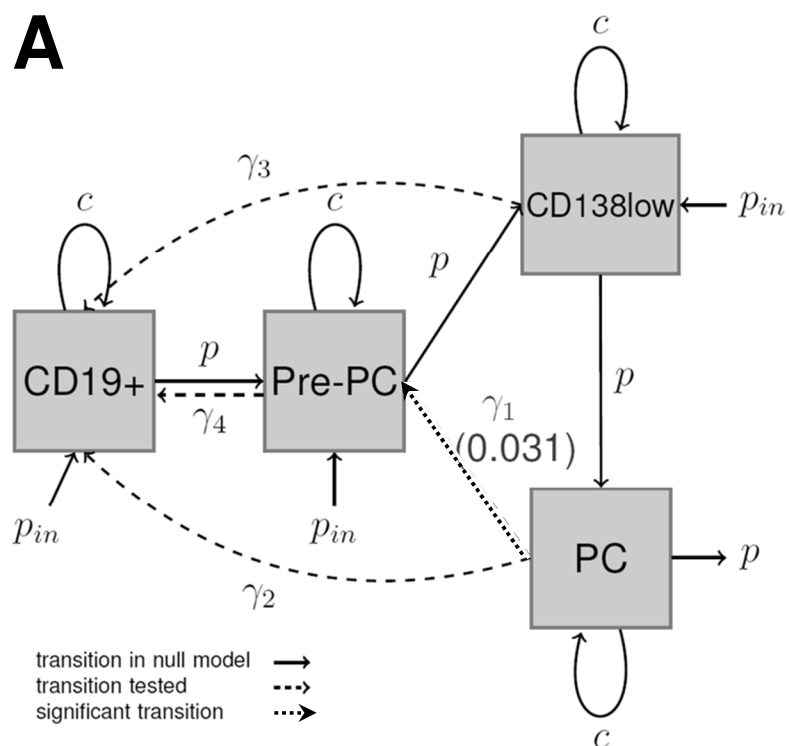
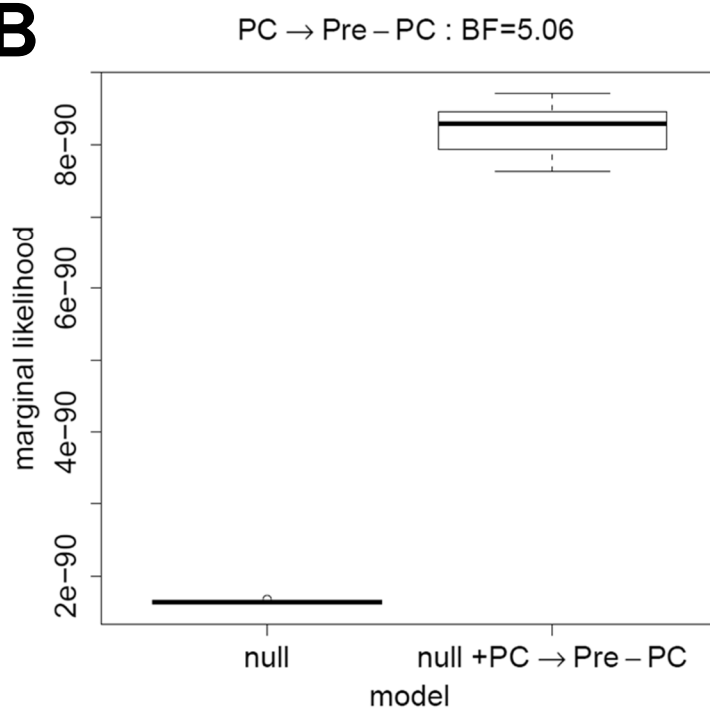


Figure 2

A**B****Figure 3**

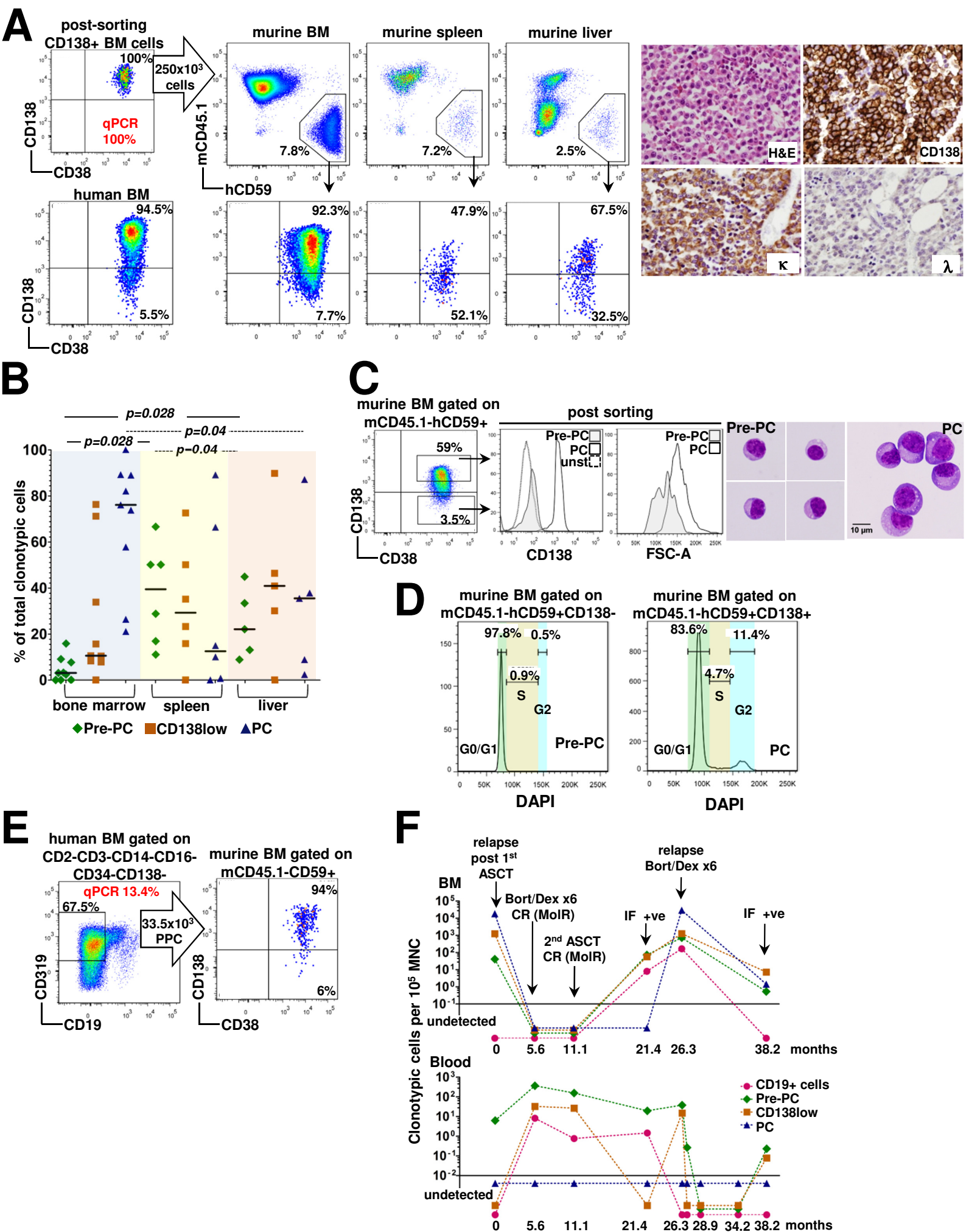
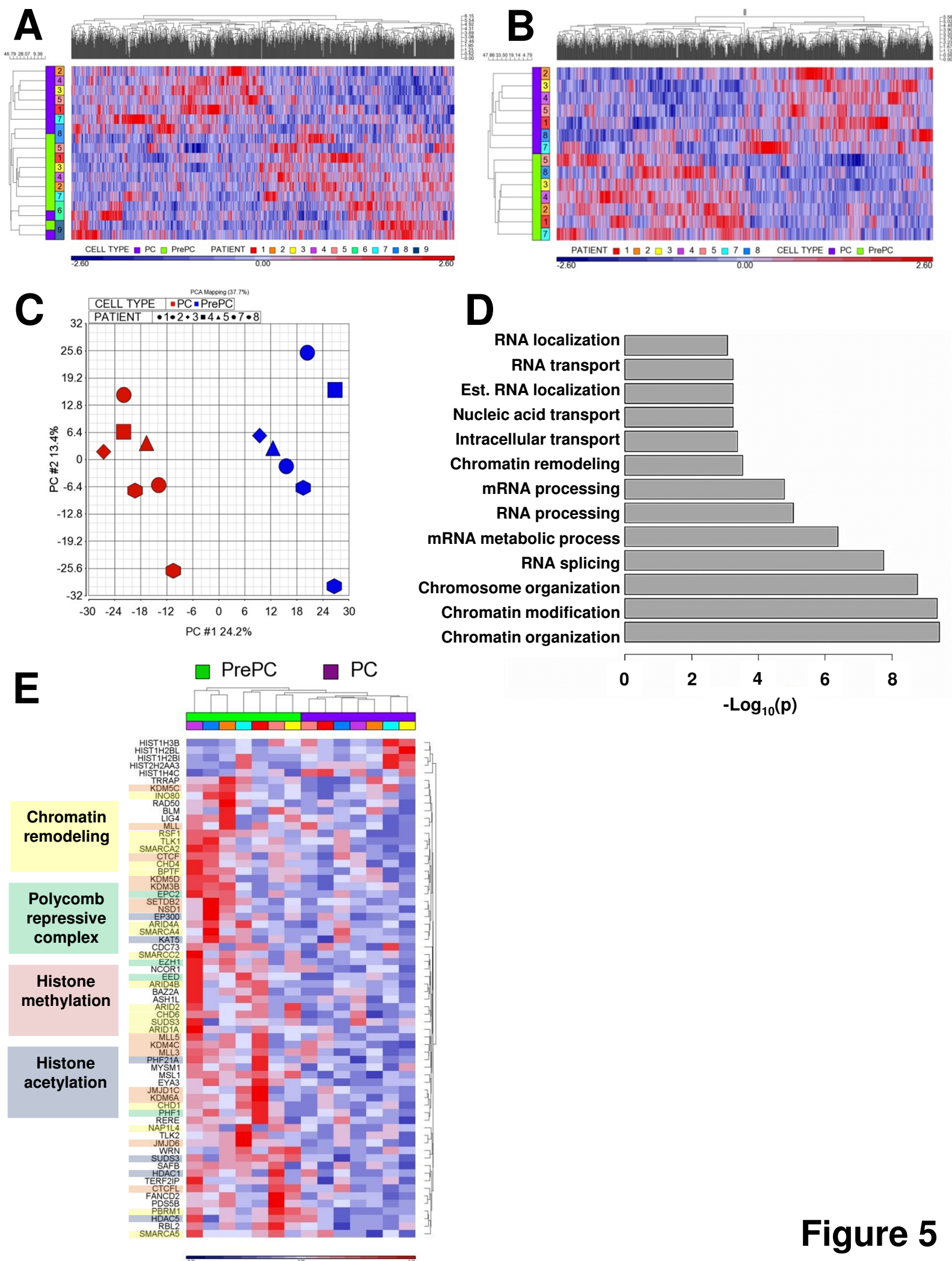


Figure 4



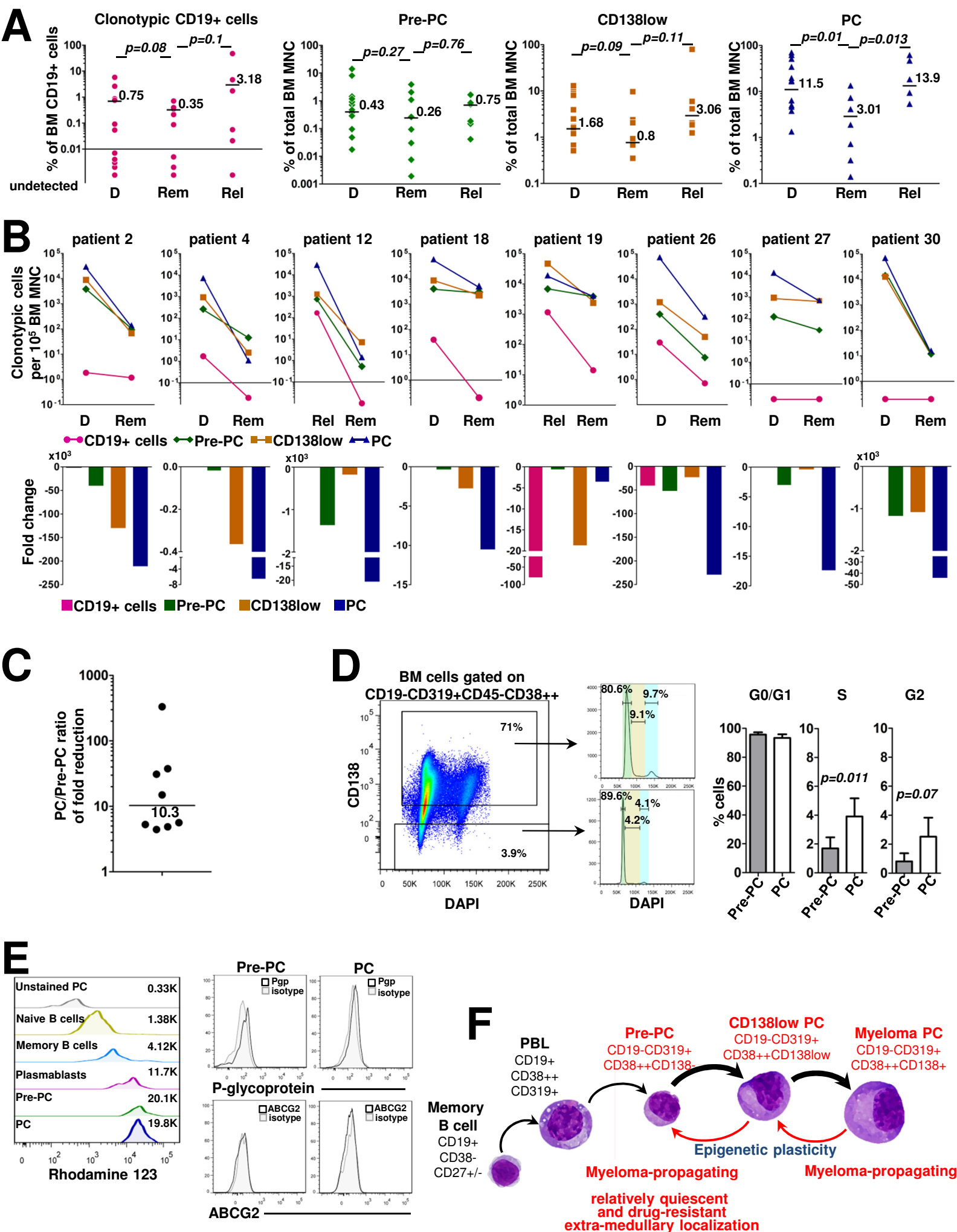


Figure 6